RSC Advances

PAPER

View Article Online
View Journal | View Issue

Cite this: *RSC Adv.*, 2015, **5**, 52629

Synthesis, structure, magnetic and photoelectric properties of $Ln_3M_{0.5}M'Se_7$ (Ln = La, Ce, Sm; M = Fe, Mn; M′ = Si, Ge) and $La_3MnGaSe_7$†

Jianqiao He,[ab] Zhe Wang,[c] Xian Zhang,[b] Ye Cheng,[b] Yu Gong,[b] Xiaofang Lai,[b] Chong Zheng,*[d] Jianhua Lin[b] and Fuqiang Huang*[ab]

Received 30th March 2015
Accepted 8th June 2015

DOI: 10.1039/c5ra05629b

www.rsc.org/advances

Six new isostructural compounds, with the formulas $La_3Fe_{0.5}GeSe_7$, $La_3MnGaSe_7$, $Ce_3Fe_{0.5}SiSe_7$, $Ce_3Mn_{0.5}SiSe_7$, $Sm_3Fe_{0.5}SiSe_7$ and $Sm_3Mn_{0.5}GeSe_7$, have been successfully synthesized *via* a molten salt method. Their structures are determined by single crystal X-ray diffraction and they crystallize in the $Ce_6Al_{3.33}S_{14}$ structure type (space group: $P6_3$, Pearson symbol: *hP*24). Pure phases of the $Ce_3Fe_{0.5}SiSe_7$, $Ce_3Mn_{0.5}SiSe_7$, $Sm_3Fe_{0.5}SiSe_7$ and $Sm_3Mn_{0.5}GeSe_7$ compounds were obtained by solid state reaction and were characterized by powder X-ray diffraction (PXRD), scanning electron microscope (SEM), ultraviolet-visible-infrared (UV-vis-IR) absorbance spectroscopy, and magnetization measurements. The $Ce_3Fe_{0.5}SiSe_7$ and $Ce_3Mn_{0.5}SiSe_7$ compounds show paramagnetic domination accompanied by antiferromagnetic contributions, while the $Sm_3Mn_{0.5}GeSe_7$ and $Sm_3Fe_{0.5}SiSe_7$ compounds show antiferromagnetic phase transitions with Néel temperatures of 13 K and 24 K, respectively. Optical measurements reveal that all of the four compounds can absorb most of visible light. These four compounds also show photoelectric properties with the photocurrent densities of 81, 1.3, 1.8 and 0.8 μA cm^{-2}, respectively.

Introduction

Designing new multicomponent compounds with unique properties or special functions is one of the important directions for modern materials science. Chalcogenides always have complex structures and rich chemical/physical properties, making them good candidates for multifunctional device applications.[1–6] Among the large family of chalcogenides, the rare earth chalcogenides have much more complex electronic configuration than the d- and p-block metal chalcogenides, resulting in their promising potentials for thermal, electrical, magnetic and optical applications.[7–16] Therefore, the discoveries of new rare earth based chalcogenides are important and intriguing.

Among the well-known rare earth chalcogenides, there is a large family of compounds ($Ln_3MM'Q_7$, Ln = lanthanide elements, M and M′ = metal or semimetal elements, Q = chalcogens) which has received increasing attention due to its richness in composition and specific optical, magnetic and ionic conducting properties.[10,13,15,17,18] The $Ln_3MM'Q_7$ compounds crystallize in the $Ce_6Al_{3.33}S_{14}$ structure type (space group $P6_3$, Pearson symbol *hP*24). This structure type can tolerate various combinations of M and M′, which provides us the capabilities to tune the properties of these compounds. The most common combinations of M and M′ are: (i) monovalent M (Na^+, Ag^+ or Cu^+) and tetravalent M′ (Si^{4+}, Ge^{4+} or Sn^{4+}),[9,11,12,15–30] (ii) divalent M (Mg^{2+}, Mn^{2+}, Fe^{2+}, Co^{2+} or Zn^{2+}) and trivalent M′ (Al^{3+}, Ga^{3+}, In^{3+} or Fe^{3+}).[31–34] These two types of combinations demand that the valence of M and M′ must sum up to 5. By introducing vacancies into the M or M′ site in the structure, new combinations such as divalent M (with 50% occupancy), trivalent M (with 33.3% occupancy) and tetravalent M′ are realized.[10,13,35,36] Therefore, the number of the compounds from the family can be enlarged. Besides, by introducing magnetic active d-block metal ions (for instance Fe^{2+}, Ni^{2+} and Mn^{2+}) to the M site, researchers can construct diverse spin–spin interactions (such as d–d, d–f or f–f interactions), which may lead to interesting magnetic properties. However, other properties of these compounds, for instance photoelectric properties, are rarely reported.[34]

Hence, in this work, we report six new rare earth selenides, containing magnetic active d-block elements (Mn, Fe) of the $Ln_3MM'Q_7$ family, namely the $La_3Fe_{0.5}GeSe_7$, $La_3MnGaSe_7$, $Ce_3Fe_{0.5}SiSe_7$, $Ce_3Mn_{0.5}SiSe_7$, $Sm_3Fe_{0.5}SiSe_7$ and

[a]*CAS Key Laboratory of Materials for Energy Conversion, Shanghai Institute of Ceramics, Chinese Academy of Sciences, Shanghai 200050, China. E-mail: huangfq@mail.sic.ac.cn*

[b]*State Key Laboratory of Rare Earth Materials Chemistry and Applications, College of Chemistry and Molecular Engineering, Peking University, Beijing 100871, China*

[c]*School of Physics and Nuclear Engineering, Beihang University, Beijing 100191, China*

[d]*Department of Chemistry and Biochemistry, Northern Illinois University, DeKalb, Illinois 60115, USA. E-mail: czheng@niu.edu*

† Electronic supplementary information (ESI) available: EDS elements ratios and solid-state UV-vis-IR diffuse-reflection spectra. CCDC 1056817–1056822. For ESI and crystallographic data in CIF or other electronic format see DOI: 10.1039/c5ra05629b

$Sm_3Mn_{0.5}GeSe_7$ compounds. These six compounds were synthesized *via* the traditional molten salt methods. Their structures were determined by single crystal X-ray diffraction. Pure phases of $Ce_3Fe_{0.5}SiSe_7$, $Ce_3Mn_{0.5}SiSe_7$, $Sm_3Fe_{0.5}SiSe_7$ and $Sm_3Mn_{0.5}GeSe_7$ were obtained through simple solid state reactions. The four samples were characterized by PXRD, SEM, UV-vis-IR absorbance spectroscopy, and magnetization measurements. In addition, the photoelectric properties of the four compounds are also investigated.

Experimental section

Synthesis

All operations were carried out in an Ar-protected glove box. The crystals are synthesized by traditional molten salt method with KI acting as flux. High purity elements and KI were mixed with the molar ratio of Ln : M : M′ : Se : KI = 3 : 0.5 : 1 : 7 : 30 (for the Si or Ge contained compounds) or 3 : 1 : 1 : 7 : 30 (for $La_3MnGaSe_7$). The mixtures were ground and sealed in carbon-coated fused silica tubes under vacuum (10^{-3} mbar). Then, the tubes were slowly heated to 1273 K in a programmable furnace followed by keeping at this temperature for 3 days. Afterwards, the tubes were slowly cooled to 773 K at the rate of 2 K h^{-1}, and then quenched in air to room temperature. The final products were obtained by carefully breaking the tubes and washed by distilled water for several times and dried by acetone to obtain red crystals of $Ce_3Mn_{0.5}SiSe_7$ and black crystals of the other five compounds. The direct combination reactions of the starting materials, without the flux (KI), were used to synthesize the powder samples.

X-ray crystallography

Single crystal data collection of each of the six compounds was carried on a Bruker Smart-1000 CCD diffractometer equipped with graphite-monochromated Mo K_α radiation at 296 K. The structure was solved with direct methods built in the program SHELXS, and refined with the full-matrix least-squares method using the SHELXL-97 program.[37] The crystal data and the structure refinement details for the compounds are summarized in Table 1. Atomic coordinates and thermal displacement factors are shown in Table 2. Selected interatomic distances are presented in Table 3.

Characterization

Powder X-ray diffractions performed on a Bruker X-ray diffractometer (Cu K_α) were used to verify the phase purity of the as-synthesized powder samples. The presence of the four elements Ln, M, M′ and Se was confirmed by energy dispersive spectroscopy (EDS) analysis on a Phenom Pro X scanning electron microscope (SEM). Optical diffuse-reflectance measurements were carried out using a UV-4100 spectrophotometer at room temperature with the scan range from 1800 nm to 300 nm. The $BaSO_4$ powder was chosen to be the 100% reflectance standard. The powder samples were ground and spread on a compacted base of $BaSO_4$ powder. The magnetic properties of the powder samples were studied by using a superconducting quantum interference device magnetometer (Quantum design, PPMS). The DC susceptibility measurements, both under zero-field-cooling (ZFC) and field-cooling (FC) conditions, were performed under a 5000 Oe magnetic field for temperatures ranging from 2 to 300 K.

Photo response properties

The powder samples were ground into fine powders before use. Then the fine powders were pressed into disks (diameter: 13 mm) under 15 MPa. Afterwards the disks were sealed in silica tubes under vacuum (10^{-3} mbar), followed by annealing at 1073 K for 2 h. Afterwards, the disks were polished to an appropriate shape (rectangular slice, size 6 × 5 × 1 mm^3) which is suitable for the measurements. The photo response measurements were performed on a Chenhua electrochemical workstation in the linear sweep voltage mode. The

Table 1 Crystallographic data and details of the structure refinement for the six compounds

Formula	$La_3Fe_{0.5}GeSe_7$	$La_3MnGaSe_7$	$Ce_3Fe_{0.5}SiSe_7$	$Ce_3Mn_{0.5}SiSe_7$	$Sm_3Mn_{0.5}GeSe_7$	$Sm_3Fe_{0.5}SiSe_7$
Formula weight	1070.21 g mol^{-1}	1094.11 g mol^{-1}	1029.08 g mol^{-1}	1028.62 g mol^{-1}	1103.98 g mol^{-1}	1059.82 g mol^{-1}
Space group	$P6_3$	$P6_3$	$P6_3$	$P6_3$	$P6_3$	$P6_3$
Unit cell	a = 10.7186(3) Å, c = 6.0797(3) Å	a = 10.5894(3) Å, c = 6.3458(3) Å	a = 10.6380(3) Å, c = 6.0079(3) Å	a = 10.6684(2) Å, c = 6.0127(2) Å	a = 10.3958(8) Å, c = 6.0175(7) Å	a = 10.4075(4) Å, c = 5.9566(4) Å
Volume	604.91(4) $Å^3$	616.25(4) $Å^3$	588.81(4) $Å^3$	592.65(3) $Å^3$	563.20(9) $Å^3$	558.76(5) $Å^3$
Z	2	2	2	2	2	2
Calculated density	4.7530 g cm^{-3}	5.8959 g cm^{-3}	4.2726 g cm^{-3}	4.2321 g cm^{-3}	4.2082 g cm^{-3}	6.4646 g cm^{-3}
Absorption coefficient	34.421	33.944	33.670	33.372	41.143	39.649
Reflections collected	1405	1560	990	1674	1121	1008
Independence reflections	719	536	376	541	995	472
Goodness-of-fit on F^2	1.026	1.124	1.101	1.093	1.008	1.006
Final R indices [$I > 2\sigma(I)$]	R_1 = 0.0454, wR_2 = 0.0947	R_1 = 0.0240, wR_2 = 0.590	R_1 = 0.0337, wR_2 = 0.0755	R_1 = 0.0260, wR_2 = 0.0607	R_1 = 0.0649, wR_2 = 0.1432	R_1 = 0.0442, wR_2 = 0.0869
R indices (all data)	R_1 = 0.0460, wR_2 = 0.0951	R_1 = 0.0255, wR_2 = 0.594	R_1 = 0.0346, wR_2 = 0.0760	R_1 = 0.0285, wR_2 = 0.0615	R_1 = 0.0685, wR_2 = 0.1461	R_1 = 0.0490, wR_2 = 0.0899
Extinction coefficient	0.013(1)	0.0039(4)	0.0049(6)	0.0013(3)	0.016(2)	0.016(1)

Table 2 Atomic coordinates for the six compounds

Compounds	Atom	Wykoff position	x/a	y/b	z/c
$La_3Fe_{0.5}GeSe_7$	La	6c	0.3567(1)	0.2266(1)	0.0357(3)
	Fe	2a	0	0	0.303(3)
	Ge	2b	2/3	1/3	0.4514(7)
	Se1	6c	0.0896(2)	0.2460(2)	0.0513(4)
	Se2	6c	0.5812(2)	0.4804(2)	0.3021(4)
	Se3	2b	2/3	1/3	−0.1681(6)
$La_3MnGaSe_7$	La	6c	0.85319(8)	0.62457(8)	0.4271(2)
	Mn	2a	0	0	0.7078(7)
	Ga	2b	2/3	1/3	−0.1568(4)
	Se1	6c	0.7576(1)	0.8537(1)	0.4694(2)
	Se2	6c	0.9075(2)	0.4261(1)	0.6993(2)
	Se3	2b	2/3	1/3	0.2170(4)
$Ce_3Fe_{0.5}SiSe_7$	Ce	6c	0.6432(1)	0.8723(1)	0.3430(3)
	Fe	2a	0	0	0.611(3)
	Si	2b	1/3	2/3	−0.246(2)
	Se1	6c	0.9123(2)	1.1585(2)	0.3584(4)
	Se2	6c	0.4153(2)	0.8933(2)	0.6132(4)
	Se3	2b	1/3	2/3	0.1299(7)
$Ce_3Mn_{0.5}SiSe_7$	Ce	6c	0.64189(7)	0.87249(7)	0.2984(2)
	Mn	2a	0	0	0.534(3)
	Si	2b	1/3	2/3	−0.116(1)
	Se1	6c	0.9119(1)	1.1607(1)	0.2857(3)
	Se2	6c	0.4783(1)	0.5855(1)	0.0320(3)
	Se3	2b	1/3	2/3	0.5149(4)
$Sm_3Fe_{0.5}SiSe_7$	Sm	6c	0.6432(1)	0.7731(1)	0.1534(4)
	Fe	2a	0	0	−0.129(3)
	Si	2b	1/3	2/3	−0.268(2)
	Se1	6c	0.8417(3)	1.0907(3)	0.1333(5)
	Se2	6c	0.4181(3)	0.5206(3)	−0.1096(5)
	Se3	2b	1/3	2/3	0.3677(8)
$Sm_3Mn_{0.5}GeSe_7$	Sm	6c	0.7755(2)	0.6424(2)	0.3606(6)
	Mn	2a	0	0	0.639(5)
	Ge	2b	2/3	1/3	0.776(1)
	Se1	6c	0.7471(4)	0.9046(4)	0.3877(8)
	Se2	6c	0.5175(4)	0.4220(4)	0.6198(9)
	Se3	2b	2/3	1/3	0.160(1)

Table 3 Selected interatomic distances (Å) for the six compounds

Atoms		$La_3Fe_{0.5}GeSe_7$	$La_3MnGaSe_7$	$Ce_3Fe_{0.5}SiSe_7$	$Ce_3Mn_{0.5}SiSe_7$	$Sm_3Fe_{0.5}SiSe_7$	$Sm_3Mn_{0.5}GeSe_7$
Ln–	Se1	2.972(2)	3.044(1)	2.950(2)	2.973(1)	2.894(3)	2.889(4)
	Se1	2.975(2)	3.072(2)	2.958(2)	2.983(1)	2.894(3)	2.914(4)
	Se1	3.123(3)	3.155(2)	3.089(3)	3.104(2)	3.023(4)	3.001(6)
	Se1	3.303(3)	—	3.264(3)	3.248(2)	3.250(4)	3.312(6)
	Se2	3.044(3)	2.989(2)	3.018(2)	3.004(2)	2.949(3)	2.955(5)
	Se2	3.138(3)	3.090(2)	3.116(2)	3.104(2)	3.040(3)	3.038(5)
	Se2	3.198(2)	3.187(2)	3.172(2)	3.179(2)	3.131(3)	3.128(5)
	Se3	3.174(2)	3.016(2)	3.176(2)	3.181(1)	3.112(2)	3.069(3)
M–	Se1	2.76(1) × 3	2.701(3) × 3	2.73(1) × 3	2.768(8) × 3	2.67(1) × 3	2.74(2) × 3
	Se1	2.77(1) × 3	2.787(3) × 3	2.75(1) × 3	2.780(8) × 3	2.75(1) × 3	2.75(2) × 3
M′–	Se2	2.365(3) × 3	2.407(2) × 3	2.276(4) × 3	2.297(3) × 3	2.306(6) × 3	2.360(5) × 3
	Se3	2.313(5)	2.372(4)	2.26(1)	2.217(7)	2.17(1)	2.31(1)

external voltage ranges from 0 V to 1 V. The visible light irradiation was conducted by a xenon lamp with the cutoff wavelength of 420 nm.

Results and discussion

Synthesis and structure description

Well-defined single crystals of the six compounds are obtained by traditional molten salt method, and their SEM images and

elements mapping are shown in Fig. 1. Elements mapping results show high degree of homogeneity and confirm the existence of the relevant elements in the corresponding compounds. Their corresponding elements ratios, with the sum formula of $La_{2.7}Fe_{0.54}GeSe_{6.52}$, $La_{2.96}Mn_{0.69}GaSe_{7.25}$, $Ce_{3.48}Mn_{0.48}SiSe_{6.8}$, $Ce_{3.27}Fe_{0.46}SiSe_{7.31}$, $Sm_{3.28}Mn_{0.51}GeSe_{7.39}$ and $Sm_3Fe_{0.48}SiSe_{6.8}$, respectively, are summarized in Table S1 in the ESI.†

The six isostructural compounds crystallize in the hexagonal space group $P6_3$ (Person symbol *hP*24), which belong to the $Ce_6Al_{3.33}S_{14}$ structure type. Their structures feature one-dimensional $[M_xSe_6]$ chains (M = Fe, Mn; $x = 0.5$ for Si or Ge containing compounds; $x = 1$ for $La_3MnGaSe_7$) and isolated $[M'Se_4]$ tetrahedrons (M′ = Si, Ga or Ge) along the 6_3 axis, as shown in Fig. 2a and b. These building blocks occupy two different channels in the 3D network formed by corner or edge sharing $[LnSe_x]$ single or double capped trigonal prisms ($x = 7$ for $La_3MnGaSe_7$; $x = 8$ for the other five compounds). It should be noted that all the $[M'Se_4]$ tetrahedrons point to the same direction along the c axis, making the structure non-centrosymmetric. The structure of $Sm_3Fe_{0.5}SiSe_7$ compound is discussed here as an example. There are one unique Sm site (6c), one unique Fe site (2a), one unique Si site (2b), and 3 unique Se sites (6c, 6c and 2b). Fig. 2c shows the coordination geometry of the Sm, Fe and Si atoms in the $Sm_3Fe_{0.5}SiSe_7$ compound. One Fe atom coordinates to six Se atoms and resides at the center of the Se_6 octahedron with nearly equal Fe–Se bond length (2.676–2.757 Å). For the five Si^{4+} or Ge^{4+} containing compounds (M^{2+} and M'^{4+} combination) the Fe^{2+} or Mn^{2+} ions half occupied the 2a sites to reach charge balance, as illustrated in Fig. 2d. The Si atom coordinates to four Se atoms to form a tetrahedron which undergoes squashed distortion along the *c* axis. The Sm atom coordinates to eight Se atoms with the average Sm–Se distance of 3.026 Å, which is comparable to the reported Sm/Se structures (Sm_2Se_3 and Sm_3Se_4).[38,39] It is worthy to note that the La atoms (in the $La_3MnGaSe_7$ compound) are seven coordinated by Se atoms with the average La–Se distance of 2.99 Å. There is another Se atom which is a little far from the La atom (3.65 Å).

Other researchers have concluded that the *c* parameter is determined by the choice of the M′ component and the effect of M is subtle.[33] This is also true for the six compounds here including the five compounds with half occupied sites. The cell parameter *c* of the two Ge containing compounds $La_3Fe_{0.5}GeSe_7$ (6.0797(3) Å) and $Sm_3Mn_{0.5}GeSe_7$ (6.0175(7) Å) are close to those of $Re_3CuGeSe_7$ (6.04–6.04 Å).[22] This is also the case for the two Si containing compounds compared with $Re_3Ag_{1-\delta}SiSe_7$.[15]

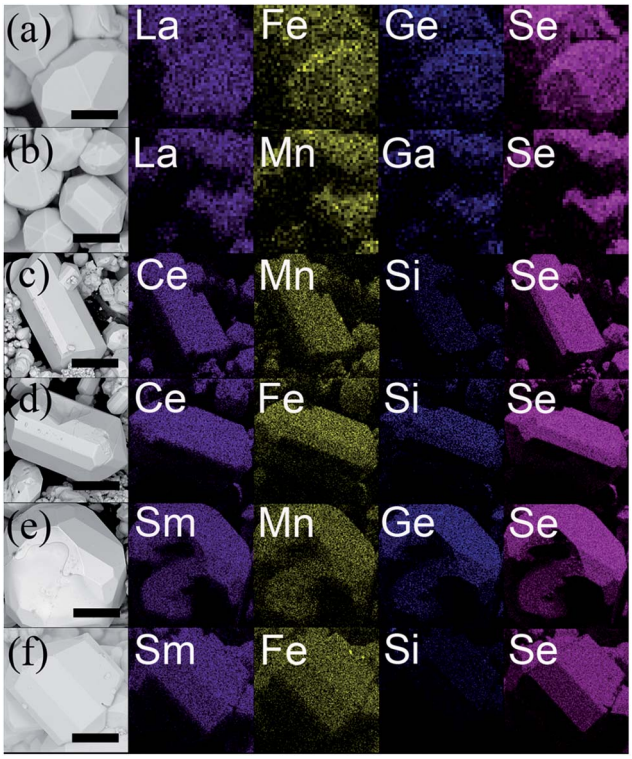

Fig. 1 SEM images and elements distributions of the single crystals of the six compounds. (a) $La_3Fe_{0.5}GeSe$, (b) $La_3MnGaSe_7$, (c) $Ce_3Fe_{0.5}SiSe_7$, (d) $Ce_3Mn_{0.5}SiSe_7$, (e) $Sm_3Mn_{0.5}GeSe_7$, (f) $Sm_3Fe_{0.5}SiSe_7$. The black bar in the picture represents a length of 20 μm.

Powder X-ray diffractions and optical properties

The pure-phase samples were obtained by re-grinding and heating of the starting materials for three times. Their phase purity was checked by PXRD, as shown in Fig. 3. The simulated pattern of $Ce_3Mn_{0.5}SiSe_7$ was also included. The six compounds have similar PXRD patterns as they are isostructural. No extra peaks are observed in the patterns of $Ce_3Fe_{0.5}SiSe_7$, $Ce_3Mn_{0.5}SiSe_7$, $Sm_3Fe_{0.5}SiSe_7$ and $Sm_3Mn_{0.5}GeSe_7$ compounds, meaning that the pure phases of the four compounds were obtained.

However, peaks corresponding to lanthanum selenides (marked with asterisks) still exist in the PXRD patterns of the

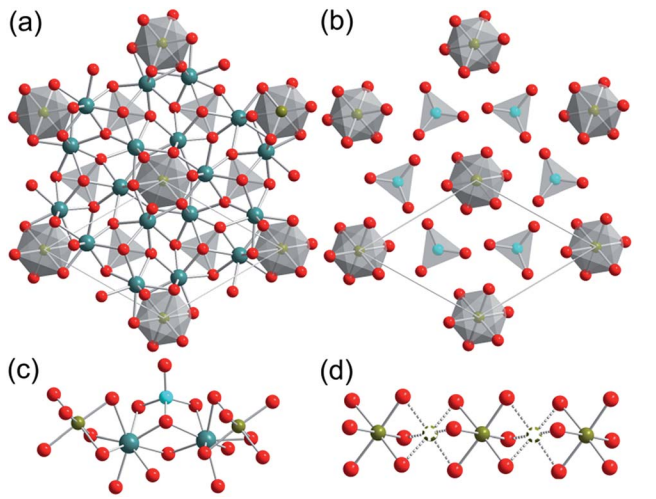

Fig. 2 (a) Schematic diagrams of the $Sm_3Fe_{0.5}SiSe_7$ structure viewed down the *c* axis. (b) The one dimensional chain of $[FeSe_6]$ octahedrons and isolated $[SiSe_4]$ tetrahedrons. Sm atoms are omitted for clarity. (c) The coordination geometry of Sm, Fe and Si atoms in $Sm_3Fe_{0.5}GeSe_7$. (d) The one dimensional chain of $[FeSe_6]$ in $Sm_3Fe_{0.5}GeSe_7$ compound. The Fe vacancies were drawn as dashed line circle. Green: Sm; Yellow: Fe; Blue: Si; Red: Se.

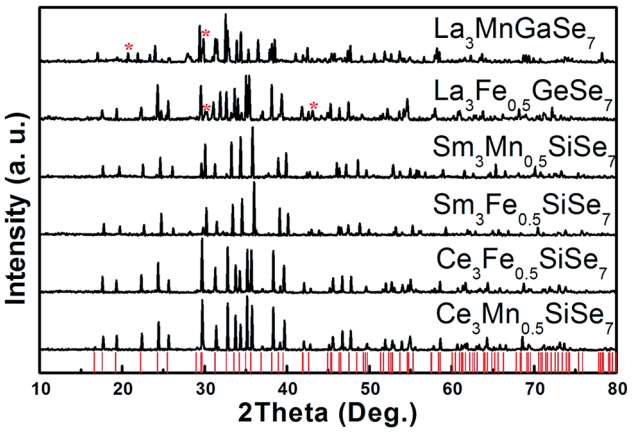

Fig. 3 The PXRD patterns of the powder samples. The red lines correspond to the theoretical patterns of $Ce_3Mn_{0.5}SiSe_7$. Peaks corresponding to lanthanum selenides are marked with asterisks.

$La_3Fe_{0.5}GeSe_7$ and $La_3MnGaSe_7$ compounds after the regrinding and heating process.

The UV-vis-IR spectra of the four pure samples are shown in Figure S1.† The band gap energies of the four compounds were estimated by using an extrapolation method, as illustrated in Fig. 4. The $Ce_3Mn_{0.5}SiSe_7$ compound has the largest band gap energy of 1.81 eV, which is consistent with its red color. The $Ce_3Fe_{0.5}SiSe_7$ compound has similar pattern to $Ce_3Mn_{0.5}SiSe_7$ compound but absorbs strongly through the whole range with a smaller band gap energy of 1.37 eV. Spectra of the two Sm containing compounds are much more complex than those of the two Ce containing compounds. A series of absorption peaks arise in the infrared region, which can be attributed to the complicated Sm^{3+} ions' 4f orbital character. The $Sm_3Fe_{0.5}SiSe_7$ and $Sm_3Mn_{0.5}GeSe_7$ compounds have small band gap energies of 1.13 eV and 1.37 eV, respectively. The two Fe containing compounds have smaller band gap energies than those of their Mn containing analogues. Theoretical calculations have found that Fe d–d and Ln f–f correlations have great impact on band gap energies of $Ln_3FeGaSe_7$ (Ln = Gd, Dy).[32] Therefore, the discrepancies between Fe and Mn d–d intra-atomic correlations may result in the differences of band gap energies between the Fe- and Mn-containing compounds. Optical measurements suggest that these materials are semiconductors and suitable for efficient absorption of solar radiation for solar cell applications.

Magnetic properties

The zero-field-cooling and field-cooling M–T curves of the four pure samples are shown in Fig. 5. In the high temperature region, all the four samples show paramagnetic behaviors, which can be attributed to both Ln and M sublattices. The inverse magnetic susceptibility are fitted by using the modified Curie–Weiss law, $\chi = C/(T-\theta_p)$. The observed total effective magnetic moments were calculated from the equation $\mu_{eff} = (4.57C)^{1/2}\mu_B$.[40] The total theoretical magnetic moments were calculated from $\mu_{eff} = [3\mu_{eff}(Ln)^2 + 0.5\mu_{eff}(M)^2]^{1/2}\mu_B$.[41,42] The Curie constant C, Weiss constant θ_p, observed and theoretical effective magnetic moments μ_{eff} are listed in Table 4.

The $Sm_3Mn_{0.5}GeSe_7$ and $Sm_3Fe_{0.5}SiSe_7$ compounds show obvious antiferromagnetic phase transitions around 13 K and 24 K, respectively. The ZFC and FC curves of the $Sm_3Fe_{0.5}SiSe_7$ compound are not coincident in the low temperature range, which may be caused by some unidentified ferromagnetic impurities. The Weiss constant θ_p of the two compounds is around −150 K indicating strong antiferromagnetic coupling interactions in the two compounds. Similar behavior has been observed in Sm_3FeGaS_7, which possesses antiferromagnetic transition around 24 K.[33] While $Sm_3Al_{0.33}SiS_7$, Sm_3CuGeS_7, $Sm_3CuGeSe_7$ and Sm_3CoGaS_7 exhibit no obvious magnetic transition and their inverse magnetic susceptibilities are curvilinear in low temperature region.[10,12,33] Fitting the inverse magnetic susceptibility to modified Curie–Weiss law in high temperature region in several cases leads to negative θ_p,

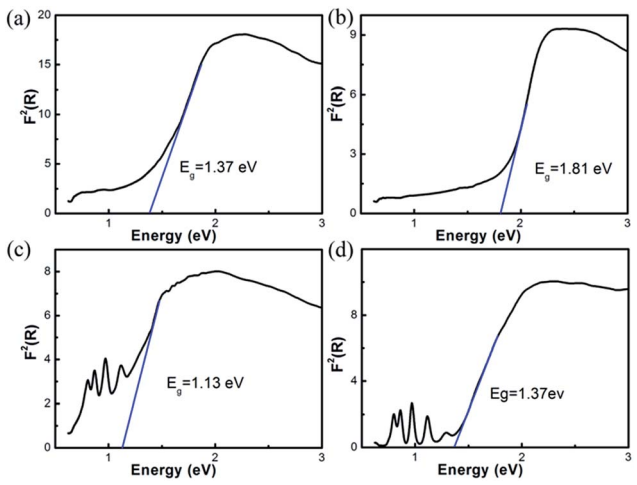

Fig. 4 The plot of $F^2(R)$ against photon energy of the four compounds: (a) $Ce_3Fe_{0.5}SiSe_7$; (b) $Ce_3Mn_{0.5}SiSe_7$; (c) $Sm_3Fe_{0.5}SiSe_7$; (d) $Sm_3Mn_{0.5}GeSe_7$.

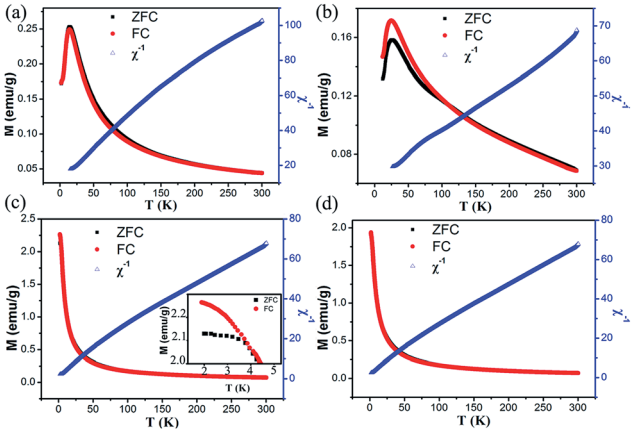

Fig. 5 Zero-field-cooling (ZFC) and field-cooling (FC) magnetization curves and the inverse susceptibility with the applied field of 5000 Oe of (a) $Sm_3Mn_{0.5}GeSe_7$, (b) $Sm_3Fe_{0.5}SiSe_7$, (c) $Ce_3Fe_{0.5}SiSe_7$, (d) $Ce_3Mn_{0.5}SiSe_7$.

Table 4 Magnetic properties of $Sm_3Mn_{0.5}GeSe_7$, $Sm_3Fe_{0.5}SiSe_7$, $Ce_3Fe_{0.5}SiSe_7$ and $Ce_3Mn_{0.5}SiSe_7$

	$Sm_3Mn_{0.5}GeSe_7$	$Sm_3Fe_{0.5}SiSe_7$	$Ce_3Fe_{0.5}SiSe_7$	$Ce_3Mn_{0.5}SiSe_7$
C (emu mol^{-1} Oe^{-1} K)	4.40	6.45	5.22	5.10
Θ_p(K)	−156.41	−143.39	−57.01	−49.50
μ_{eff} (μ_B) obs	4.48	5.43	4.88	4.83
μ_{eff} (μ_B) theory	4.9	4.33	5.41	5.89

indicating weak antiferromagnetic coupling interactions dominant in these compounds.

The $Ce_3Fe_{0.5}SiSe_7$ and $Ce_3Mn_{0.5}SiSe_7$ compounds are paramagnetic over the entire temperature range from 2 K to 300 K as clearly showed by the linear behavior of the inverse magnetic susceptibility. This is similar to the magnetism of Ce_3NiGaS_7.[33] ZFC and FC curves of $Ce_3Fe_{0.5}SiSe_7$ separates from each other below 4 K (see the insert of Fig. 5c) indicating that the sample may contain some unknown ferromagnetic impurities. The Weiss constant θ_p for the two compounds is around −50 K, indicating antiferromagnetic coupling interactions. Among the other Ce containing compounds, Ce_3FeGaS_7 and Ce_3CoGaS_7 show non Curie–Weiss behavior; $Ce_3CuSnSe_7$ exhibits antiferromagnetic transition around 5 K.[9,33] The effective magnetic moments of the four compounds are close to their expectations.

It is reported that La_3MAlS_7 (M = Mn, Fe, Co) exhibit linear antiferromagnetism due to short-range ordering in the [MS_6] octahedron chains, which is characterized by a broad maximum around 115–130 K in the magnetic susceptibility.[31] However, such antiferromagnetic transition has rarely been seen in other $Ln_3MM'Q_7$ compounds.[32,33,36] It is believed that antiferromagnetic coupling interactions are dominant in this series of compounds, but long-range ordering is only manifested in a few cases, which could be assigned to the moments localized on the Ln^{3+} ions.[9,33] Therefore, the antiferromagnetic phase transitions observed in $Sm_3Mn_{0.5}GeSe_7$ and $Sm_3Fe_{0.5}SiSe_7$ compounds are likely due to Sm^{3+} moments. The absence of antiferromagnetic transition in $Ce_3Fe_{0.5}SiSe_7$ and $Ce_3Mn_{0.5}SiSe_7$ compounds is not surprising as it is similar to the case in other Ce containing $Ln_3MM'Q_7$ compounds.[33] To shed more light on the magnetic behaviors of the compounds studied, neutron diffraction measurements are still needed.

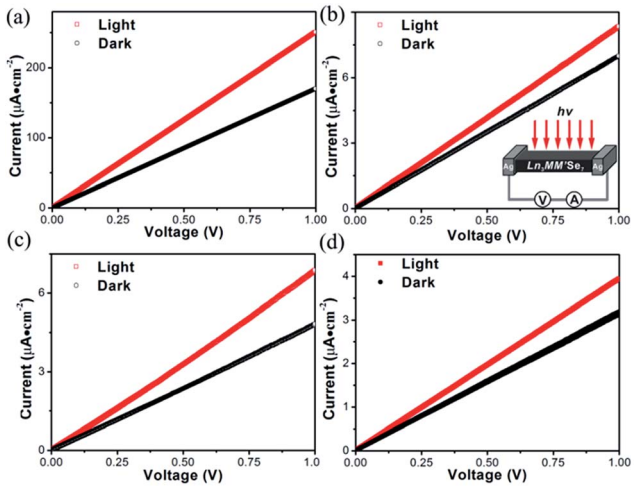

Fig. 6 Current–voltage curves under dark and visible light irradiation of (a) $Ce_3Fe_{0.5}SiSe_7$, (b) $Ce_3Mn_{0.5}SiSe_7$, (c) $Sm_3Fe_{0.5}SiSe_7$, (d) $Sm_3Mn_{0.5}GeSe_7$.

Photo-response properties

The powder samples of the four pure samples were pressed into slices, while the silver paste was dropped onto the two sides of the slices to form the photo-response devices (Fig. 6b inset). The photo response properties of the four pure samples were measured at room temperature, and the current–voltage (I–V) curves are shown in Fig. 6a–d. The dark current density of the $Ce_3Fe_{0.5}SiSe_7$, $Ce_3Mn_{0.5}SiSe_7$, $Sm_3Fe_{0.5}SiSe_7$ and $Sm_3Mn_{0.5}GeSe_7$ samples are 169.3, 7.0, 4.7 and 3.15 μA cm^{-2} respectively, indicating the conductivity of the four compounds. The Fe containing compounds have larger dark current densities than those of the Mn containing analogues due to their better conductivity. This is in line with the early report that La_3FeFeS_7 has smaller activation energy than La_3MnFeS_7.[31] While visible light (with a cutoff of 420 nm) illumination was conducted perpendicular to the slices, the increases of their currents were observed with photo current densities of 81, 1.3, 1.8 and 0.8 μA cm^{-2} under external voltage of 1 V for $Ce_3Fe_{0.5}SiSe_7$, $Ce_3Mn_{0.5}SiSe_7$, $Sm_3Fe_{0.5}SiSe_7$ and $Sm_3Mn_{0.5}GeSe_7$ compounds, respectively. The Photo current densities of the two Fe containing compounds are larger than that of the Mn containing analogues, which may be attributed to the smaller band gap of the Fe containing compounds than that of the Mn containing analogues. Photo response is rarely seen in $Ln_3MM'Q_7$ compounds. The only report is that $La_3CuGaSe_3$ possesses photo current density of 2.9 mA under 0.4 V.[34] The small current densities of the four tested compounds comparing to that of $La_3CuGaSe_3$ may be attributed to their high resistivity and high vacancy concentrations.

Conclusions

In summary, $La_3Fe_{0.5}GeSe_7$, $La_3MnGaSe_7$, $Ce_3Fe_{0.5}SiSe_7$, $Ce_3Mn_{0.5}SiSe_7$, $Sm_3Fe_{0.5}SiSe_7$ and $Sm_3Mn_{0.5}GeSe_7$ crystallize in the $Ce_6Al_{3.33}S_{14}$ structure type. One dimensional face sharing [MSe_6] (M = Fe, Mn) octahedron chain and isolated [$M'Se_4$] (M′ = Si, Ge, Ga) tetrahedrons occupy two different channels in the 3D network formed by Ln (Ln = La, Sm, Ce) and Se atoms. Pure phases of $Ce_3Fe_{0.5}SiSe_7$, $Ce_3Mn_{0.5}SiSe_7$, $Sm_3Mn_{0.5}GeSe_7$ and $Sm_3Fe_{0.5}SiSe_7$ were obtained through simple solid state reaction and their physical properties were measured. UV-vis-IR

spectra show that the band gap energies of $Ce_3Fe_{0.5}SiSe_7$, $Ce_3Mn_{0.5}SiSe_7$, $Sm_3Fe_{0.5}SiSe_7$ and $Sm_3Mn_{0.5}GeSe_7$ compounds are 1.37, 1.81, 1.13 and 1.37 eV, respectively. Magnetization measurements show that the four pure phases are all antiferromagnetic ($Ce_3Fe_{0.5}SiSe_7$ and $Ce_3Mn_{0.5}SiSe_7$ are paramagnetic, and the minus Weiss constants suggest that the dominant exchange interactions are antiferromagnetic) and $Sm_3Fe_{0.5}SiSe_7$ and $Sm_3Mn_{0.5}GeSe_7$ have T_N of 24 K and 13 K. Slices of $Ce_3Fe_{0.5}SiSe_7$, $Ce_3Mn_{0.5}SiSe_7$, $Sm_3Fe_{0.5}SiSe_7$ and $Sm_3Mn_{0.5}GeSe_7$ compounds show photo responses with current densities of 81, 1.3, 1.8 and 0.8 μA cm^{-2} under an external voltage of 1 V, respectively.

Acknowledgements

This work was financially supported by "Strategic Priority Research Program (B)" of the Chinese Academy of Sciences (Grant XDB04040200), Innovation Program of the CAS (Grant KJCX2-EW-W11), NSF of China (Grants 91122034, 51125006, 51202279 and 61376056), Science and Technology Commission of Shanghai (Grants 13JC1405700 and 14520722000).

Notes and references

1 T. K. Todorov, O. Gunawan, T. Gokmen and D. B. Mitzi, *Prog. Photovoltaics*, 2013, **21**, 82–87.
2 Y. Pei, X. Shi, A. LaLonde, H. Wang, L. Chen and G. J. Snyder, *Nature*, 2011, **473**, 66–69.
3 H. S. P. Wong, S. Raoux, S. Kim, J. Liang, J. P. Reifenberg, B. Rajendran, M. Asheghi and K. E. Goodson, *Proc. IEEE*, 2010, **98**, 2201–2227.
4 X. Zhang, J. He, W. Chen, C. Wang, C. Zheng, J. Lin, X. Zhang and F. Huang, *RSC Adv.*, 2014, **4**, 34288.
5 G. Zhang, B. Zhang, H. Chen, X. Zhang, C. Zheng, J. Lin and F. Huang, *J. Alloys Compd.*, 2014, **591**, 6–10.
6 X. Zhang, J. He, W. Chen, K. Zhang, C. Zheng, J. Sun, F. Liao, J. Lin and F. Huang, *Chem.–Eur. J.*, 2014, **20**, 5977–5982.
7 F. Q. Huang, P. Brazis, C. R. Kannewurf and J. A. Ibers, *J. Am. Chem. Soc.*, 2000, **122**, 80–86.
8 F. Q. Huang, W. Choe, S. Lee and J. S. Chu, *Chem. Mater.*, 1998, **10**, 1320–1326.
9 L. D. Gulay, D. Kaczorowski and A. Pietraszko, *J. Alloys Compd.*, 2005, **403**, 49–52.
10 S.-P. Guo, G.-C. Guo, M.-S. Wang, J.-P. Zou, G. Xu, G.-J. Wang, X.-F. Long and J.-S. Huang, *Inorg. Chem.*, 2009, **48**, 7059–7065.
11 I. Hartenbach, T. Nilges and T. Schleid, *Z. Anorg. Allg. Chem.*, 2007, **633**, 2445–2452.
12 O. M. Strok, M. Daszkiewicz, L. D. Gulay and D. Kaczorowski, *J. Alloys Compd.*, 2010, **493**, 47–49.
13 Y.-F. Shi, Y.-k. Chen, M.-C. Chen, L.-M. Wu, H. Lin, L.-J. Zhou and L. Chen, *Chem. Mater.*, 2015, **27**, 1876–1884.
14 G. B. Jin, E. S. Choi, R. P. Guertin, C. H. Booth and T. E. Albrecht-Schmitt, *Chem. Mater.*, 2011, **23**, 1306–1314.
15 M. Daszkiewicz, L. D. Gulay, O. S. Lychmanyuk and A. Pietraszko, *J. Alloys Compd.*, 2009, **467**, 168–172.
16 M. Daszkiewicz, L. D. Gulay, A. Pietraszko and V. Y. Shemet, *J. Solid State Chem.*, 2007, **180**, 2053–2060.
17 K. M. Poduska, F. J. DiSalvo, K. Min and P. S. Halasyamani, *J. Alloys Compd.*, 2002, **335**, L5–L9.
18 M. Daszkiewicz and L. D. Gulay, *Mater. Res. Bull.*, 2012, **47**, 497–499.
19 M. Daszkiewicz, L. D. Gulay, O. S. Lychmanyuk and A. Pietraszko, *J. Alloys Compd.*, 2008, **460**, 201–205.
20 L. D. Gulay, O. S. Lychmanyuk, I. D. Olekseyuk, M. Daszkiewicz, J. Stepien-Damm and A. Pietraszko, *J. Alloys Compd.*, 2007, **431**, 185–190.
21 L. D. Gulay, O. S. Lychmanyuk, M. Wolcyrz, A. Pietraszko and I. D. Olekseyuk, *J. Alloys Compd.*, 2006, **425**, 159–163.
22 L. D. Gulay, O. S. Lychmanyuk, I. D. Olekseyuk and A. Pietraszko, *J. Alloys Compd.*, 2006, **422**, 203–207.
23 L. D. Gulay, O. S. Lychmanyuk, J. Stepien-Damm, A. Pietraszko and I. D. Olekseyuk, *J. Alloys Compd.*, 2005, **402**, 201–203.
24 L. D. Gulay and I. D. Olekseyuk, *J. Alloys Compd.*, 2005, **388**, 274–278.
25 L. D. Gulay, V. Y. Shemet and I. D. Olekseyuk, *J. Alloys Compd.*, 2005, **388**, 59–64.
26 L. D. Gulay, I. D. Olekseyuk, M. Wolcryz and J. Stepien-Damm, *Z. Anorg. Allg. Chem.*, 2005, **631**, 1919–1923.
27 F. Q. Huang and J. A. Ibers, *Acta Crystallogr., Sect. C: Cryst. Struct. Commun.*, 1999, **55**, 1210–1212.
28 S. J. Hwu, C. K. Bucher, J. D. Carpenter and S. P. Taylor, *Inorg. Chem.*, 1995, **34**, 1979–1980.
29 S. H. Lin, J. G. Mao, G. C. Guo and J. S. Huang, *J. Alloys Compd.*, 1997, **252**, L8–L11.
30 O. S. Lychmanyuk, L. D. Gulay, I. D. Olekseyuk, J. Stepien-Damm, M. Daszkiewicz and A. Pietraszko, *Pol. J. Chem.*, 2007, **81**, 353–367.
31 K. S. Nanjundaswamy and J. Gopalakrishnan, *J. Solid State Chem.*, 1983, **49**, 51–58.
32 W. Yin, W. Wang, L. Kang, Z. Lin, K. Feng, Y. Shi, W. Hao, J. Yao and Y. Wu, *J. Solid State Chem.*, 2013, **202**, 269–275.
33 B. W. Rudyk, S. S. Stoyko, A. O. Oliynyk and A. Mar, *J. Solid State Chem.*, 2014, **210**, 79–88.
34 X. Zhang, W. Chen, D. Mei, C. Zheng, F. Liao, Y. Li, J. Lin and F. Huang, *J. Alloys Compd.*, 2014, **610**, 671–675.
35 R. L. Gitzendanner, C. M. Spencer, F. J. DiSalvo, M. A. Pell and J. A. Ibers, *J. Solid State Chem.*, 1997, **131**, 399–404.
36 M. Daszkiewicz, O. V. Marchuk, L. D. Gulay and D. Kaczorowski, *J. Alloys Compd.*, 2014, **610**, 258–263.
37 G. Sheldrick, 1997.
38 N. Y. Pribyl'skaya, A. A. Eliseev, N. Y. Pribyl'skii and R. S. Gamidov, *Russ. J. Inorg. Chem.*, 1984, **29**, 451–452.
39 R. B. Beeken and J. W. Schweitzer, *Phys. Rev. B: Condens. Matter Mater. Phys.*, 1981, **23**, 3620–3626.
40 C. J. Oconnor, *Prog. Inorg. Chem.*, 1982, **29**, 203–283.
41 C. Kittel, *Introduction to solid state physics*, 5th edn, 1976.
42 H. Schmid, H. Rieder and E. Ascher, *Solid State Commun.*, 1965, **3**, 327–330.